引用格式：Muhammad Bilal, TIAN Zhenyu. Recent Development and Applications of Particle Image Velocimetry from Laboratory to Industry (Invited)[J]. Acta Photonica Sinica, 2023, 52(3):0352103
Muhammad Bilal,田振玉.粒子图像测速技术:从实验室到工业应用的进展(特邀)[J].光子学报,2023,52(3):0352103

粒子图像测速技术:从实验室到工业应用的进展(特邀)

Muhammad Bilal[1,2],田振玉[1,2]
(1 中国科学院工程热物理研究所, 北京 100190)
(2 中国科学院大学, 北京 100049)

摘 要:粒子图像测速(PIV)已成为测量流体流动速度场的重要实验技术。该方法产生瞬时流型的定量表示,通常用于帮助构建复杂流动的现象学模型和数值模拟验证。PIV分析可广泛用于实验流体力学等多个研究领域。两步处理法,即自相关和互相关,已被用于检查时空流演化,可以实现作为空间分辨率函数的涡度测量和精度估计。PIV的发展与测量流场的复杂性和难度逐渐增加紧密相关。用于测量的PIV技术发展迅速,并呈现出新的趋势,主要体现在立体PIV、断层PIV、大型PIV、微型PIV、3D PIV、行人PIV以及使用高时间/空间分辨率设备。PIV在医学研究、能源燃料、燃烧、流场测量、实时过程监测、结构变形、灌溉、声学、地质学、海洋学、水资源、林业、人群监测和采矿矿物加工等各种研究领域有着广泛的应用。本文对实验室PIV发展进行全面概述,通过在工业过程和日常生活中采用PIV进行实时监控,讨论了PIV如何以精确的时间分辨率和特殊分辨率取代现有的分析成像技术。此外,还综合比较了数值模拟和目前可用的PIV分析技术。

关键词:粒子图像测速;过程监控PIV;PIV的应用;流场测量;人群监测
中图分类号:O359 **文献标识码**:A **doi**:10.3788/gzxb20235203.0352103

0 Introduction

Particle Image Velocimetry (PIV) originated with the strengthening of the laser speckle velocimetry technique. PIV was first reported in 1984 and distinguished as the capability to capture discrete particle images instead of densely overlapping particle speckle patterns[1]. In the past four decades, PIV has become an important and widely used means of performing near-instantaneous and non-intrusive flow visualization measurement techniques. The establishment of the laser speckle velocimetry method was initially used for solid mechanics and later on used for fluid flow visualization[2-5].

The PIV technique involves seeding the flow with tracers that are capable to follow the dynamic behavior of the flow. High-intensity light sources (lasers, LEDs, etc.), such that a camera focused on the desired measurement field of view can capture them with illuminate tracers. At least two consecutive images separated by a time delay are sufficient to observe the motion of particles. It can use long sequences of consecutive images to give information about the temporal flow. However, two-pulse PIV is the most popular (time-resolved PIV). It can calculate the flow velocity using the known light pulse delay and cross-correlation analysis of the captured images[6-7].

Foundation item: National Science and Technology Major Project (No. J2019-III-0005-0048), Ministry of Science and Technology of China (Nos. 2021YFA0716200/2022YFB4003900), Natural Science Foundation of China (Nos. 51976216, 51888103, 52161145105/M-0139), Beijing Municipal Natural Science Foundation (No. JQ20017), Chinese Academy of Sciences (Nos. YJKYYQ20210006, GJTD-2020-07), CAS-TWAS Scholarships
First author: Muhammad Bilal, bilal@iet.cn
Contact author: TIAN Zhenyu, tianzhenyu@iet.cn
Received: Oct.26,2022; **Accepted**: Dec.14,2022

PIV has been used to solve a wide range of flow issues, from the flow over an aircraft wing in a wind tunnel to the production of vortices in prosthetic heart valves. Though less prevalent, PIV can also measure the motion of solid materials, deformation, and tissues that include embedded markers or those that are visibly diverse in some other manner.

Despite much interest in PIV, there are only limited reviews summarizing what it had done so far in this field. Most of them focused on either reviewing engineering imaging, aerodynamics, flow field, combustion measurements, stereoscopic and micro-PIV. To the best of our knowledge, there have been scarce literature reviews that comprehensively discuss industrial the aspects of PIV. This review mainly focused on the comprehensive overview of the development of PIV in the laboratory which needs to be implemented in industry and daily life by monitoring the real-time process for better understanding. This will lead to fast industrial processing as well as health. Using PIV to replace current analytical imaging techniques with enhanced temporal and special resolution has been discussed. In addition, it also provided a comparison of numerical simulation and previously available analytical techniques with PIV.

1 Techniques/instruments

A variety of PIV configurations can be used depending on the flow component requirements. The development of PIV is linked to the gradual increase in the complexity and difficulty of measured flow fields. PIV techniques for measurements have developed significantly, and new trends have emerged. The key developments are stereoscopic PIV, tomographic PIV, large-scale PIV, micro PIV, 3D PIV, pedestrian PIV and using high-temporal/spatial-resolution devices. The recent development of PIV in various areas extends autonomously, as seen by a spider web graph in Fig. 1 which indicates the independent development in each subfield of PIV, connected circles of the web indicate the supportive development in any component/subfield of PIV support to all fields of PIV. The basic and most common method is planer PIV, in which a thin laser sheet illuminates, and the camera captures two events of fluid flow motion over a plane. Other methods, such as

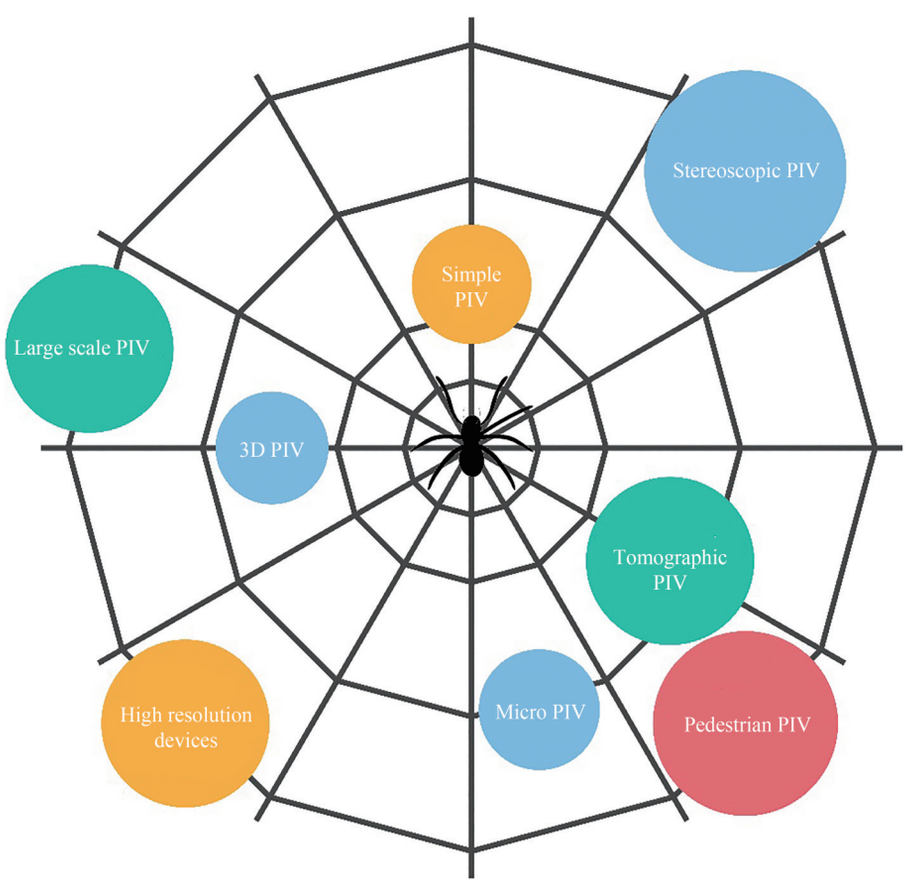

Fig. 1 Development of PIV

stereoscopic PIV, use two inclined cameras focusing on the same plane, allowing all three components of fluid flow motion in that plane to be extracted[8-16]. Echo particle image velocimetry (echo-PIV) can acquire two-dimensional velocity fields in optically opaque fields for applications in biological and industrial flow[17-18]. The more advanced tomographic PIV technique requires an illuminated volume of interest, where multiple cameras from different directions capture the three-dimensional (3D) construction of flow velocities[19-23]. Although various other PIV configurations exist, however planer PIV method is common.

For early measurements of the PIV technique used continuous lasers, photographic film cameras, and optical Fourier transforms using Young's fringes for displacement analysis. Modern PIV systems use high-energy pulsed laser systems, digital cameras capable of capturing from individually each laser pulse, and a computer-based cross-correlation technique. Typically, flow tracers comprise fine chemical or oil sprays (such as di-ethyl-hexyl-sebacate, better known as DEHS) used in gaseous flows and hollow glass spheres in water flows are common.

1.1 Lasers

High-power pulsed laser systems are common in PIV measurements to freeze particle motion, precisely control image exposure, and achieve the required illumination intensity. Nd:YAG (neodymium-doped yttrium aluminum garnet) laser systems are commonly used in two and multi-pulse PIV experiments, typically in a frequency-doubled arrangement to generate visible 532 nm wavelength light output. The laser pulse intervals demanded in many PIV experiments are too short for successive pulses from single cavity Nd:YAG systems, therefore PIV lasers usually comprise two laser cavities (one for each laser pulse), with beam combining optics for co-alignment of each beam. Two timing signals are required for the operation of each laser cavity, first triggering the flashlamp, which excites the system and builds the energy within the laser cavity, followed by the Q-switch, which allows the energy release in a concentrated pulse using an electro-optical device known as a Pockels cell. An optimal delay exists between the flashlamp and Q-switch triggering to enable maximum laser energy output. Repetition rates of these systems are typically 10~15 Hz, with laser pulse energies over 400 mJ/pulse. MATT S et al[24] use a Litron ND:Yag laser and high frequency CCD camera to visualize the effect of optical turbulence and density gradients on PIV. Fig. 2(a) shows the concept of PIV measurements. Fig. 2(b) shows the PIV system configured for a measurement plane with a path length of around 1 m. They positioned the mirror such that the light sheet (green laser, wavelength 532 nm) projected into the tank at a 90-degree angle to illuminate a cross section. They point the camera at the bottom edge, but for the experiments mentioned in this paper, they set the camera up to look at the tank's center height.

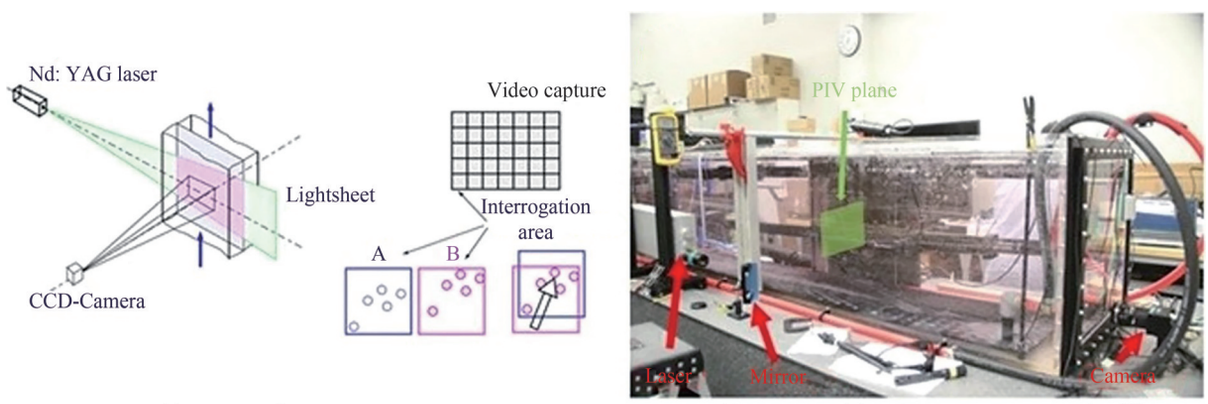

(a) Concept of PIV measurements (b) 1-meter path length PIV measurement plane[24]

Fig. 2 Concept of PIV measurements and 1-meter path length PIV measurement plane[24]

After emission from the laser system, a series of optics manipulates the laser beam to control the illumination of the measurement field of view. In planar and stereoscopic PIV, a thin laser light sheet is required to isolate particles, which are generated using a combination of negative and positive focal length optics. FILATYEV S et al[25] used stereo PIV and double-pulsed planar laser-induced fluorescence to study turbulent premixed flames. In the double pulsed PIV mode, a spectra-physics quanta-ray PIV 400-10 Nd:YAG laser was employed for illumination. ZHANG Z et al[26] employed a high-speed double cavity Nd:YLF laser as the

light source and two high-speed CMOS cameras to study the flow field of momentum-driven pulsed transient jets using time-resolved PIV.

1.2 Cameras

Nowadays, in PIV technique used a Charge-Coupled Device (CCD) or Complementary Metal-Oxide-Semiconductor (CMOS) sensors, having the capability of capturing at least two consecutive frames with minimal separation time. A "frame straddling" technique is often used to minimize the delay between successive PIV images, timing the first laser pulse at the end of the camera's first exposure, and the second laser pulse at the beginning of the second exposure.

LEWANDOWSKI B et al[27] used a high-speed CMOS camera had a resolution of 1 280×1 040 pixels with a frequency of 300 Hz, polyamide seeding particles with an average diameter of 20 μm in water illuminated by a continuous laser of wavelength 532 nm to analyze wake structures in bubbly flows. While DENG K et al[28] utilize PIV with an intensified Charge-Coupled Device (ICCD) on the combustion instability of Hydrogen-Methane lean premixed swirling flames affected by acoustic excitation.

KAUFER T et al[29] use low-cost action cameras to produce stereoscopic PIV measurements. A continuous wave laser or a Light-Emitting Diode (LED) provided the illumination. The action cameras (GoPro Hero 5) used an image sensor with a pixel size of 1.55 μm×1.55 μm and delivered a single picture over time to films with a frame rate of up to 240 Hz.

1.3 Tracer particles

The choice of tracer particles is critical since the velocity field can be measured using the PIV approach by detecting the displacement of the tracer particles. Tracers depend on the measurement of the flow field. Common demand for good tracers should be visible, chemically inert, appropriate in size can follow the flow, and be environment friendly. High signal-to-noise ratio obtainment requires good particle dispersion and optical scattering. Current publications present a variety of tracers depending on the application.

Silicate powders or mono dispersed metallic oxides such as SiO_2, Al_2O_3, TiO_2 and ZrO_2 are commonly used in combustion PIV experiments as seeding particles. Because SiO_2 has a low melting point but excellent scattering, Al_2O_3 has a high melting point but poor scattering, and TiO_2 has a higher melting point but better scattering, ZrO_2 is a potential option for ultrahigh temperature PIV[30-32].

Silver-coated hollow glass spheres and glass beads were employed as a tracer for liquid field flow. DAGHRAH M et al[33] employed silver-coated hollow glass spheres with diameters ranging from 9 to 14 μm as a tracer for PIV measurements of oil flow within disc-type transformer winding radial cooling ducts. AHMADI F et al[34] use glass beads of size 285 μm to 700 μm in diameter to measure a horizontal channel flow.

Previous research has used median filters, main orientation filters, and maximum filters, but these methods aren't stable enough due to a lack of concern for both tracer particle visibility and stability. Tracer visibility cannot be predicted by statistical properties like Signal-to-Noise Ratio (SNR) and peak cross-correlation. As far as image matching is concerned, they suggest a robust and effective filter called Peak-Peak-Sidelobe-Ratio (PPSR) to ensure tracers' visibility and stability. Testing the proposed method on Brenta and Tiber is used to demonstrate its efficacy[35].

1.4 Optical imaging

A digital camera takes two or more consecutive PIV images, which are divided into small patches and cross-correlated. A normalized cross-correlation scheme is applied to each interrogation window to project particle displacement based on the shift in the correlation peak from the window's center. After the displacement of each interrogation window has been estimated, these values are spatially recompiled to produce an array of velocity vectors describing the measured flow. A turbulent buoyant jet discharging in a linearly stratified environment, CLEMENT S A et al[36] employ multi spatio-temporal scales PIV. Steps were also tuned to capture global characteristics while resolving space and time locally on the Kolmogorov scale.

1.5 Software or analysis system

Key developments in PIV to date have come from improvements to the experimental data. While frequent enhancements to the way processing algorithms handle PIV data have resulted in dramatic improvements to the quality of PIV results. The treatment of PIV image interrogation windows was an area of early development,

where iterative correlation schemes enabled the progressive refinement of displacement estimates and increased the spatial resolution of results. The multi-pass method applies an iterative correlation procedure, whereby displacement estimates from earlier correlation iterations determine integer window offsets to one (or both) of the images in a PIV image pair during subsequent correlation "passes". This method was first implemented by establishing window offset estimates for the second image using a forward differencing interrogation scheme[37]. They later introduced a central differencing interrogation technique, applying symmetric window offsets in both the first and second images[38]. Introducing the so-called multi-grid approach further leveraged the iterative correlation passes to enable progressive refinement of the interrogation grid to smaller interrogation window sizes, increasing spatial resolution[39-40]. This technique bypassed prior limitations on final interrogation window size because of large relative particle displacements. Window and image deformation schemes extended these techniques with sub-pixel deformation of a PIV image to correct for local velocity gradients. This approach was first proposed by HUANG H et al (1993)[41], and developed in the works of JAMBUNATHAN K et al (1995)[42] and SCARANO F (2001)[40].

Implementing sub-pixel correlation peak detection using a functional fit, often a three-point Gaussian has resulted in further improvements in the performance of each interrogation window correlation[7, 43]. They also showed interrogation window weighting to increase correlation quality by reducing biasing and aliasing effects[39, 44]. The Correlation Error Correction technique introduced by HART D P (2000) applies small shifts to interrogation windows, and they combined the resulting correlations using element-wise multiplication[45]. This method suppresses random errors and further boosts correlation signal-to-noise ratios, enabling smaller interrogation windows to be used in PIV processing. ERGIN F G[46] presents an automated static masking approach based on PIV image ensembles, which can be employed after background removal.

1.6 Limitations of technique/lasers/cameras

Although PIV is a powerful tool for flow examination, it has some major drawbacks. First, PIV measurement systems are frequently limited to a single block of optical pathways, especially for full-scale models. The problem of light obstruction could be resolved by using transparent materials, but this will make it more difficult to maintain the thermal boundaries. Furthermore, transparent material obstructions inside the models may change the optical paths and distort the particle images. Second, due to insufficient laser intensity, low spatial resolution, and limited space to expand the optical light sheet, commercial PIV often has a limited measurement area. Since this critical limitation restricts PIV applications in full-scale models, it is important to build a large-scale optical system and camera shooting technology to overcome this limitation. The PIV systems used in indoor environments have so far been noncommercial, using HFBS as tracer particles and conventional light or expanded laser light sheets for illumination.

A PIV system is also expensive, bulky, and complex to operate. A considerable investment in equipment, time, and experimental know-how is needed to accurately quantify the PIV of the indoor flow field. Anemometers with conventional sensor technology are more practical for many engineering applications, particularly for in situ measurements. In order to extend indoor PIV applications, portable and easy-to-use PIV systems are needed.

Beyond the optical sensor's nominal resolution, significant improvements were made in PIV displacement measurement by using a sub-pixel interpolation-based variety of image processing techniques. Sub-pixel interpolation of the correlation planes e.g. the Gaussian interpolation[43], the peak centroid (center-of-mass) method[47-48], a sinc interpolation[49-50], or a polynomial interpolation[51], which reduced the effect-"peak locking" or "pixel locking"[49, 52-55]. Windowing functions, at the boundaries of the interrogation area, become zero[56-57], particle image truncation reduction effect is correlated at the edges of the image interrogation areas[58]. Direct correlation with a normalization, which further realizes in three ways: asymmetrically, correlation of small interrogation area from the first image to the large area in the second image[41, 53, 59-60], symmetrically, same sized two interrogation areas[61-62], bi-directional, the combination of asymmetric direct correlation and with a small interrogation area second direct correlation from the second image correlated with a large area in the first image[58]. Iterative shift and deformation of the observed areas[63-67] or image deformation[42, 62, 68-71] with various image interpolation schemes like bi-linear interpolation which is commonly used, or higher-order more advanced method.

To achieve the desired accuracy, NOBACH H et al[72] worked on the correlation-based displacement estimation due to the intensity variation effect. In both PIV exposures, the intensity fluctuates, and certain particles get brighter between the two exposures illustrated. Fig. 3(a) indicates individual particle intensity of first exposure. Fig. 3(b) indicates individual particle intensity of the second exposure. Furthermore, errors were measured using several PIV processing methods, with bi-cubic spline or Whittaker image interpolation emerging as the best way, whereas bi-linear interpolation performed worse than the conventional FFT method. Although the Gaussian low-pass filter picture interpolation performs well without intensity changes, it has a large RMS error when compared to other approaches.

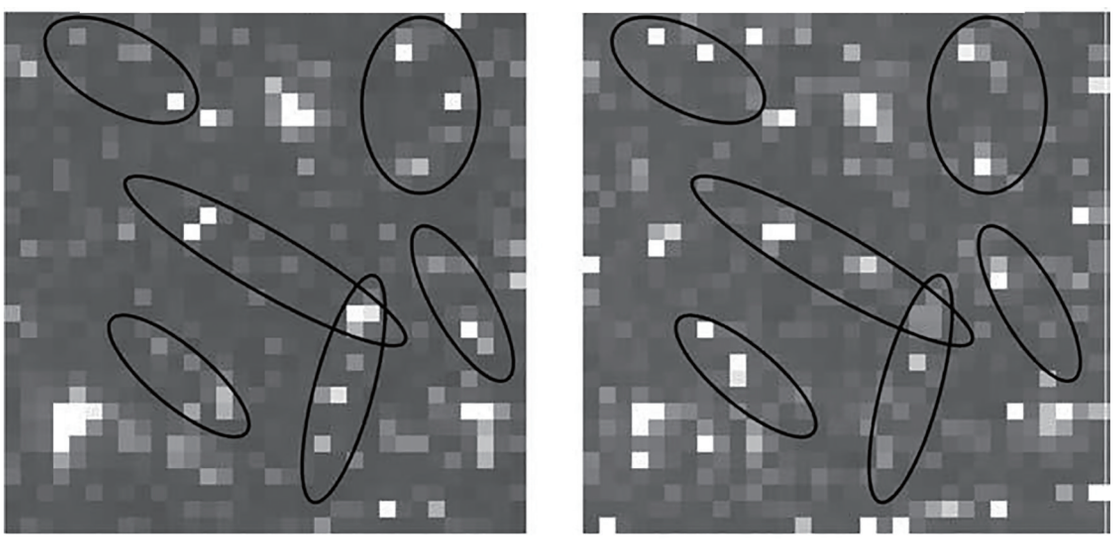

Fig. 3 Individual particle intensity variations

1.7 Accuracy or uncertainty

The parameters which affect the uncertainty include particle image size, velocity gradients, intensity and density, interrogation window size, turbulent fluctuations, and noise level. First, it must take errors because of the alignment of the apparatus and installation into consideration. Second, errors are because of system components. If a synchronizer controls the pulse delay in the light source and uses long cables, which produce some delay in laser pulses or recording systems, it could eliminate this kind of error by observing light pulses using a fast diode on an oscilloscope. Finally, errors caused by the flow itself can produce measurement errors owing to particle slip in turbulent flows with massive flow and severe velocity variations[73].

PIV error assessment and velocity ensemble measurement correction were described by NOGUEIRA J et al[74]. In addition to error assessment, this model allows for the measurement correction of statistical ensembles such as the local velocity Root Mean Square (RMS) and the local velocity average.

2 Applications

With the development of PIV systems including lasers, cameras, and analysis algorithms, now PIV may replace almost every experimental flow visualization technique around humans. PIV can visualize quantitative *in-situ* measurements in engineering, combustion, blood flow, fluid mixers, microfluidic devices, and many more. Since its invention, PIV as a nonintrusive, accurate, reliable, convenient, and powerful experimental technique for flow diagnostics, has played a highly important role in the fundamental studies on fluid dynamics, a wide range of industrial applications, understanding a variety of natural phenomena, and even exploring some flow characteristics in the body of human beings. The widely shown applications of the PIV technique may range from very low-speed flows to supersonic flows, as shown in Table 1, from flows in a nano/micro-scaled passage to flows at a large scale, like a river. Further Fig. 4 summarizes the applications of PIV according to the type and components used.

Table 1 PIV applications

Sr. No.	Application	Type of PIV	References
1	Energy fuels and combustion	Simple PIV	[10, 23, 75-82]
2	Flow field measurement	Simple PIV, μPIV, Large scale PIV, Tomographic PIV	[83-87]
3	Real-time process monitoring	μPIV, Large scale PIV, Simple PIV	[88-94]
4	Structure deformation	μPIV, Simple PIV	[95-96]
5	Irrigation	Large scale PIV	[97-100]
6	Medical applications	μPIV	[16-18, 21, 101-108]
7	Acoustics	Simple PIV	[109-117]
8	Geology	Large scale PIV	[118-121]
9	Oceanography and water resources	Large scale PIV	[9, 15, 119-120, 122-133]
10	Forestry	Simple PIV	[134-138]
11	Film radio television	Pedestrian PIV	[139-140]
12	Mining mineral processing	Simple PIV	[75, 141-142]

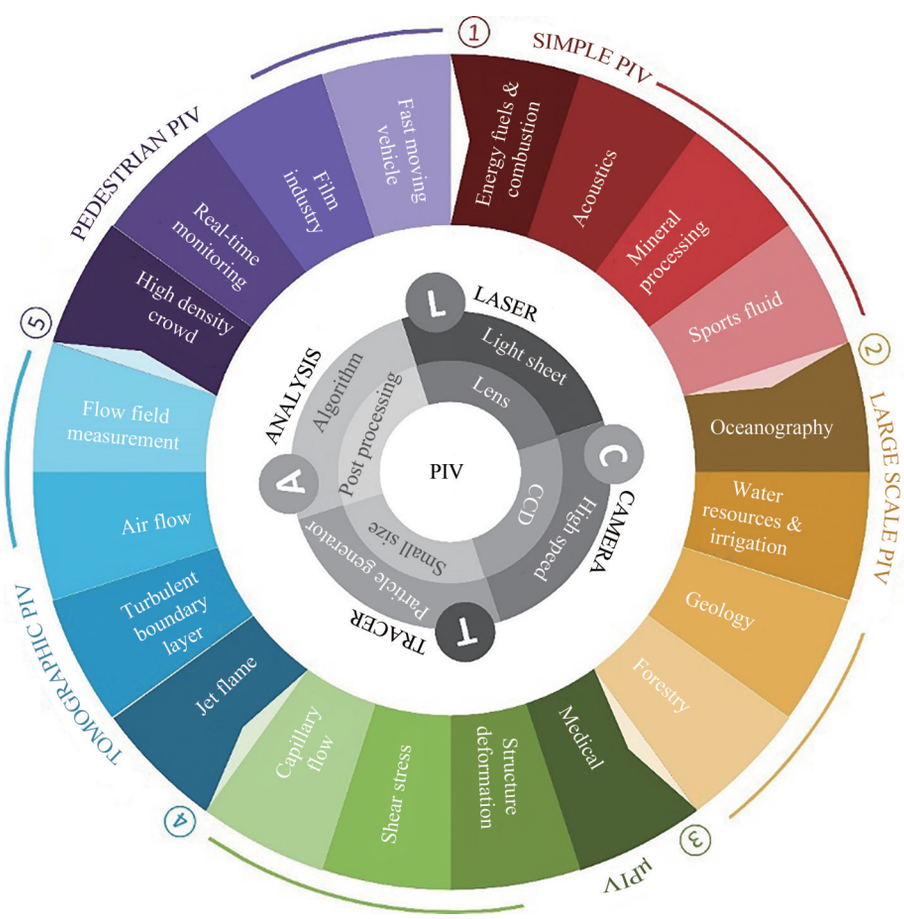

Fig. 4 Components and applications of PIV

2.1 Energy fuels and combustion

Automobile manufacturers are concerned about pollution and fuel consumption. For a variety of reasons,

including the constant rise in fuel prices and the application of strict laws, reduced consumption and emissions are especially important. As a result, continual and substantial research is necessary to meet these objectives.

BRADLEY D et al[76] used the PIV approach to determine the laminar burning velocities and Markstein numbers of methane, *i*-octane, ethanol, and *n*-butanol during flame propagation in spherical explosions. For PIV measurements, a light sheet with a thickness of 0.5 mm was illuminated in the center of the explosion chamber by a cylindrical lens using a double pulsed Nd: YAG laser (DM60-DH, Photonics) with a pulse energy of 12 mJ operating at a 532 nm wavelength at a 5 kHz frequency. A high-speed camera records images of 1 024×1 024 pixels at a frequency of 5 kHz fitted perpendicular to the laser sheet with a macro-Nikon lens of 108 mm focal length. To minimize the flame luminosity effect, an optical band-pass filter centered at 532 nm was coupled with a lens. Six jet atomizers (9010F0021, DANTEC) were used to generate olive oil droplets at a boiling temperature of 570 K and a size of less than 1 μm as seeding and tracking the flame. At atmospheric pressure, the range of equivalence ratios and a range of pressures for *n*-butanol were employed to measure burning velocities and Markstein numbers. By comparing results, PIV underestimates about 12% of Markstein′s numbers when measuring flame. FAN L et al[143] experimentally measure two-phase flow velocity by Laser-Induced Incandescence Particle Image Velocimetry (LII-PIV). Fig. 5(a) shows the mean velocity field obtained with 1 μm alumina (left half) and 0.2 μm WC (right half) for the same air jet. Fig. 5(b) shows the velocity profiles extracted and compared at h=15, 25, 35 mm.

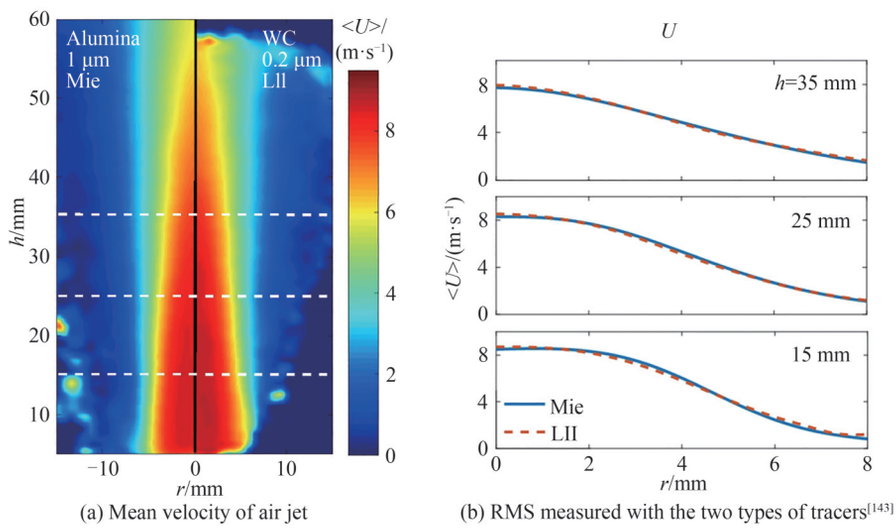

(a) Mean velocity of air jet (b) RMS measured with the two types of tracers[143]

Fig. 5 Laser-induced incandescence particle image velocimetry

BREND M A et al[77] employed stereoscopic PIV volumetric measurements in annular gas turbine combustors for port flow properties. The stereoscopic PIV system, with a central rotating stage facility, was integrated into the annular facility. They installed two cameras in the back-scatter-back-scatter configuration to capture the laser sheet, and the whole PIV system was moveable circumferentially. The PIVTec PIVPart 45 seeder was used to seed diethyl hexyl sebacate droplets of less than 1 m to the test flow region. The results found that the high levels of turbulence generated by secondary jets suggest increased momentum flux as compared to the primary port jets.

ZHANG B et al[23] investigated the non-premixed combustion parameters by deflection tomography and PIV technique measurements simultaneously. The PIV system contains a solid-state pulsed Nd: YAG laser operating at 532 nm wavelength, 15 Hz frequency, 430 mJ pulse energy, and 8 ns pulse duration to illuminate and achieve a light sheet. A cylindrical lens was used to make a 1 mm thick light sheet. To record PIV images with a digital CCD camera (Nikon 630090 Power View 4MP-LS) of 2 360×1 776 pixel resolution, both the camera and the laser are triggered through a synchronizer with an error of 1 ns. TiO_2 particles of a diameter of 5 μm were used as tracer particles and preloaded into the particle mixer. The deflection tomography system contains a continuous wave He-Ne laser of 10 mW power and 632.8 nm wavelength, a CCD camera, two Ronchi gratings, and other optical components.

2.2 Flow field measurement

The two basic approaches for studying flow fields are experimental measurements and numerical simulations. Typically, experimental measurement is difficult and time-consuming. Numerical simulation can offer both global and detailed flow quantities in a variety of applications at a low cost, which is extremely useful for system design and evaluation. However, doing a numerical simulation always need exact measurements as the boundary conditions. Simulated results cannot be completely trusted until they are validated by high-quality experimental data. Therefore, experimental measurements are still a necessary and fundamental step in flow field investigations.

TOMBUL H et al[83] used PIV data in computational intelligence models, such as Support Vector Machines (SVM) and Artificial Neural Networks (ANNs) to estimate velocity and direction in multi-phase flows. Data obtainment was tested experimentally from an eccentric pipe configuration and trained the system by Support Vector Regression (SVR), SVM, linear regression, nonlinear regression, and feed-forward neural network models for direction and velocity measurement. They recorded video data at three angles: 15°, 30° and 0° of wellbores through a digital camera. The SVM model was the best estimator for direction estimation, while the SVR model was the best for velocity estimation. KOKMANIAN K et al[144] investigated the flow field dynamics of transonic shock buffet using PIV. Fig. 6 shows the instantaneous streamwise velocity field, Fig. 6(a) u with the shock at the points where the stream turns upstream and Fig. 6(b) u with the shock at the points where the stream turns downstream. The cyan line showed where the observed shock occurred.

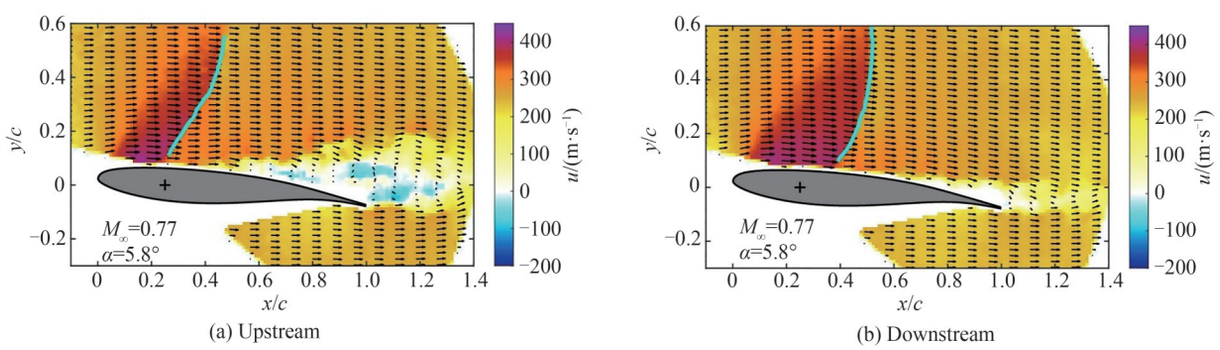

Fig. 6 Instantaneous streamwise velocity field[144]

SEO H et al[145] investigate the flow and turbulence characteristics of a bubbly jet with a low vacancy percentage experimentally. They examined the phase separation using Planar Laser-Induced Fluorescence (PLIF) and PIV. Diluted bubbly jets have fewer Reynolds shear stresses and normal stresses than pure jets, buoyant jets, bubbly jets, and bubbly plumes.

For quantitative measurements of complex flow fields, the PIV technique has been expanded from the measurement of a two-dimensional plane to three dimensions or three components with multiple camera angles. The development includes holographic PIV, stereoscopic PIV, and tomographic PIV, among others.

2.3 Real-time process monitoring

VARON E et al[88] use real-time PIV data to study the dynamics of a completely turbulent wake. Using a typical 7 Hz PIV setup and homemade software, the two-dimensional two-component (2D-2C) velocity fields were obtained. Seeding oil droplets, which were used as a tracer, were injected into the wind tunnel, which was illuminated by a double pulsed Nd: YAG laser (Twins BSL Quantel) of 200 mJ per pulse energy light sheet used. To capture two consecutive frames, the double-frame camera (PowerView Plus 4MP TSI) was connected through Bayonet Neill Concelman (BNC) connectors to the laser supply with a programming-controlled synchronization module.

2.4 Structure deformation

SAXTON-FOX T et al[95] use the PIV technique to investigate the deformation of the coherent structure in a turbulent pipe flow because of a spatially variable pressure gradient. With including a rotating body in the center of the pipe, a spatially varying pressure gradient was applied, and it carried PIV measurements in the axial-radial plane for different bodies of rotation. To illuminate the field, a green-colored laser sheet was used,

while to capture consecutive frames, two digital cameras were used. To improve the image quality near the walls, they used a rectangular box filled with water to encase the pipe. By computing two-point correlations centered at different axial locations, coherent structures were quantified. In the accelerating region, a pattern of decreasing area while increasing area in the recovery region was observed.

KWAK T Y et al[146] use the PIV technique to estimate the shear band properties and the evolution of deformation and special distribution in clayey soil from the initial to the post-failure condition. PIV was used to measure the deformation and displacement of soil particles by collecting digital photographs through a transparent side wall. They performed plane strain tests on regularly consolidated and over-consolidated clay specimens. They performed PIV image analyses using the commercial software GeoPIV. The findings reveal the properties of shear bands seen in clay, which can predict failure behavior and guide reinforcing at the actual site's soft ground locations. SATO K et al[147] also use PIV to investigate huge deformation ground with wall movement or a shallow foundation under extremely low confining pressure. For validation, numerical analysis was used to forecast fracture process zones, which were then compared to experimental PIV image analysis data.

2.5 Irrigation

In irrigation open channel bends, the existence of complex flow patterns plays an essential role in ecological and alluvial processes. Secondary flows are created by curvature when the centrifugal force and the pressure gradient caused by water surface tilting strike a balance. These secondary flows act to reduce conveyance capacity, increase energy loss, enhance mass mixing, shape bar-pool topography, alter sediment transport, and redistribute the bulk velocity of the channel[100, 148-150].

BAI R et al[98] used two-dimensional PIV to study the evolution of secondary flows in a U-shaped open channel bend with long straight input and outflow velocities. In the PIV setup, a continuous wave laser of wavelength 532 nm having a power of 8 W was used to illuminate the flow field with a thickness of 1 mm, spherical polyamide particles having a mean diameter of 5 μm as seed particles with a density of 1.03×10^3 kg/m^3. They captured particle images using a high-speed CMOS camera with a frame rate of 500 Hz and an 8-bit custom resolution of 2 560×1 920 pixels. Before approaching the curve, the flow redistributes, and it takes a significant distance to re-establish uniform conditions after passing the bend. Complex secondary flow patterns were discovered at the bend. TAURO F et al[151] utilized Large-Scale Particle Image Velocimetry (LSPIV) and Particle Tracking Velocimetry (PTV) to observe streamflow from cameras set up side the Brenta River. Fig. 7

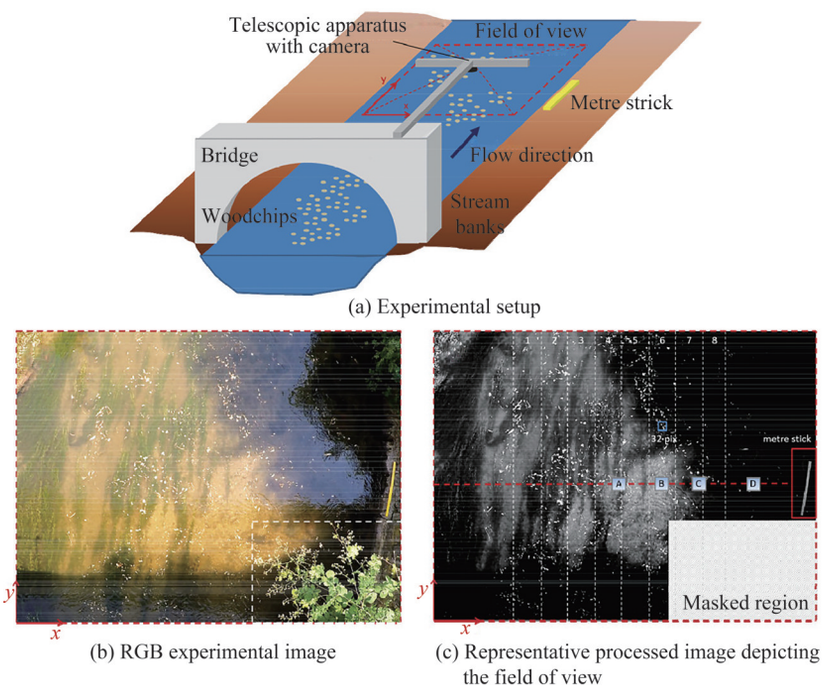

Fig. 7 View of Brenta River[151]

shows the view of Brenta River (a) experimental setup, (b) RGB experimental image, (c) representative processed image depicting the field of view.

YOON J S et al[99] suggested a system for collecting municipal trash by installing a dust collector separately and a screen in drainage canals since drainage canals cannot use a dust collector. To test the efficiency of hydraulic model tests and Large Scale PIV (LS-PIV) technique. For LS-PIV, styrofoam floating particles were inserted into the upstream part of the drainage canal. They analyzed the most effective collection at an installation angle of 15° and a blade angle of 30°.

Al-Muhammad et al[97] use micro-particle image velocimetry (Micro-PIV) experimentally and the RSM Simulation for drip irrigation to investigate the vortex zones along a labyrinth milli-channel. The 2D-2C Micro-PIV double pulsed laser (Litron Nd:YAG) source with a second harmonic (wavelength 532 nm) having a pulse energy of 135 mJ was used as an illumination source. To record the PIV images, the Dantec Dynamics HiSense 4M camera has a special resolution (2 048×2 048 pixels). They equipped this camera with a Canon MPE 65 mm $f/2.8$ lens. For two data sets, the time delay between two laser pulses was 12 μs and 6 μs.

2.6 Medical

CORTELLESSA G et al[152] investigated the SARS-CoV-2 proximity interaction between a speaking infected individual and a susceptible subject and offered an integrated risk assessment. In a three-dimensional transient numerical model, exhaled a speaking person disseminated droplets. They also performed PIV measurements to verify a computational model of the spread risk of the coronavirus illness of 2019 (COVID-19). They observed that the contribution of big droplets to the danger is hardly visible only at distances far below 0.6 m and that it declines to nil for distances longer than that, where it solely depends on flying droplets.

AVELAR A et al[101] investigated leaflet flutter using the PIV technique capabilities in biological prosthetic heart valves. They study the performance of porcine and bovine pericardium valves by simulating the cardiac flow and recording high-speed videos with a camera to quantify the cusp oscillations by using PIV to measure shear stresses and velocity profiles for the relationship with flutter. There was found to be a lower velocity value in cusps that shows no flutter, but they found no relationship between leaflet vibrations and shear stress values.

HO W H et al[102] employed additive manufacturing (3D printing) to build a Rigid Refractive-Indexed-Matched Flow Phantom on cerebral aneurysms and measured flow field velocities using the PIV method. To fabricate a flow model or phantom in biomedical fluid dynamics using desired materials and shapes, 3D printing allows printing any structure from a CAD design to a phantom using a desktop computer and 3D printer. The PIV open-source MATLAB code PIVlab 1.4.1[104, 153] cross-correlation results were consistent when compared to previous results within the aneurysm.

LI Y et al[103] presented the pilot testing of a Computational Fluid Dynamics (CFD) model in intracranial aneurysms treated with flow-diverting stents in comparison to the PIV experimental results of haemodynamics. The PIV experiment was carried out on three distinct cross-sections of a Flow Diverting (FD) stent at three different arterial flow rates (150, 250, and 400 mL/min). The PIV system (Intelligent Laser Applications, Germany) was used to illuminate the observing region using a 120 mJ Nd:YAG laser with a 532 nm wavelength, a CCD camera with a resolution of 1 280×1 024 pixels to capture images, and Rhodamine B fluorescent seeding particles with an average size of 18 μm. At various arterial flow rates and cross-sectional planes, PIV and CFD were compared qualitatively and quantitatively with and without the Silk FD stent.

ROLOFF C et al[21] compared simulation and experimental CFD vs PIV (standard, stereoscopic, and tomographic) vs phasecontrast MRI in an intracranial aneurysm for better treatment planning because of the rupture risk of intracranial aneurysms. Due to the high modeling assumptions and constraints, doctors cannot rely solely on numerical procedures for validation, hence experimental methods are required. An internal carotid artery aneurysm was studied *in-vitro* using Phase-Contrast Magnetic Resonance Imaging (PC-MRI), standard PIV, stereoscopic (sPIV), tomographic (tPIV), and Computational Fluid Dynamics (CFD) modeling in a patient-specific silicone phantom model under steady flow circumstances[107, 154-159]. To calculate a Similarity Index (SI) for each approach, they used velocity vectors and mean velocity magnitude variances across all participating modalities. Compared to all experimental techniques, PC-MRI experienced differences and was unable to estimate overall velocity magnitude levels inside the vessel because of the limited resolution. Fig. 8(a) shows the 3D flow pattern generated from CFD simulation. Fig. 8(b) shows the comparison of 2D magnitude of

the x- and y-velocity components acquired by PIV, sPIV, tPIV, PC-MRI, and CFD. Fig. 8(c) shows the comparison of the three-dimensional velocity magnitude acquired by PIV, tPIV, PC-MRI, and CFD in these six cut planes.

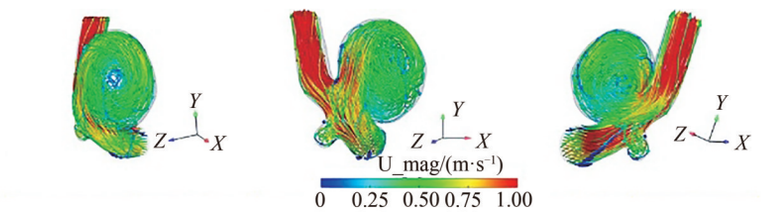

(a) 3D flow pattern generated from CFD simulation

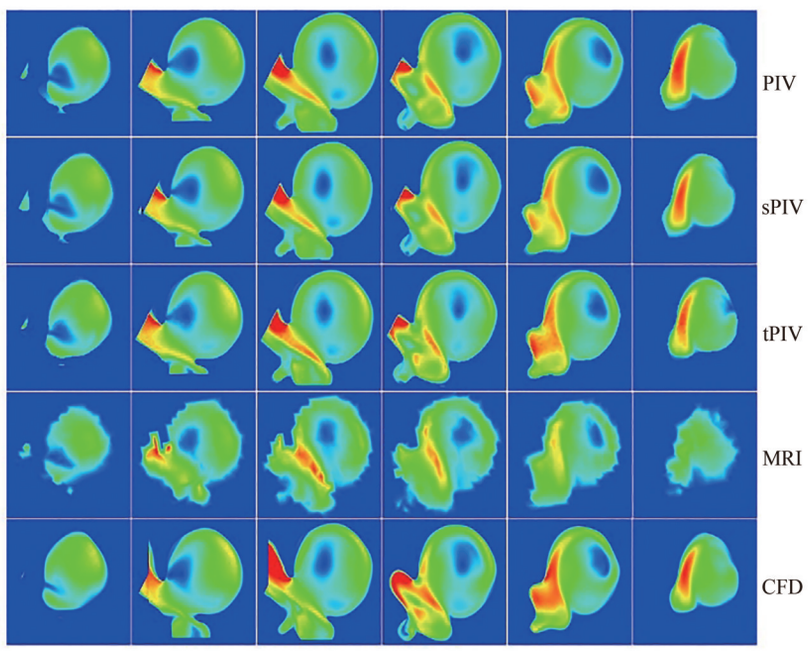

(b) Comparison of 2D magnitude of the x- and y-velocity components acquired by PIV, sPIV, tPIV, PC-MRI, and CFD

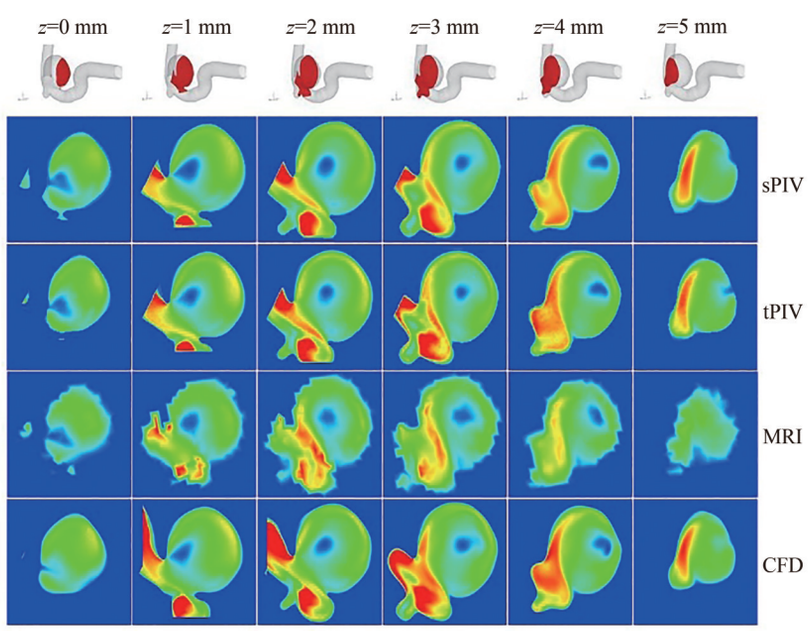

(c) Comparison of the three-dimensional velocity magnitude acquired by PIV, tPIV, PC-MRI, and CFD in these six cut planes

Fig. 8 Results in Ref. [21]

2.7 Acoustics

LIOU Y S et al[111] investigated the flow induction phenomena of acoustic force, acoustic streaming, and Ultrasonic Standing Wave (USW) by PIV, microparticle tracking velocimetry (PTV), and Flow Visualization (FV). PMMA (Poly(methyl methacrylate)) cuvettes were studded with acoustic streaming and USW to control particle aggregation in suspension solutions. They generated the flow using a piezoelectric plate working with a voltage signal oscillating at a MHz frequency. They filled the cuvette with water and a suspension solution of μm-size particles. USW is generated inside the liquid due to oscillation, while the confined space induces acoustic streaming flow at the same time. A continuous laser (Blue Sky Tec Co., Ltd) with a power of 40 mW and a wavelength of 532 nm was used to illuminate the test assembly, and a green-colored laser beam with a diameter of 2 mm was used to expand as a light sheet with a cylindrical lens. A high-resolution camera (Zyla 5.5 sCMOS, ANDOR) was used to record the images. The observed results revealed USW used acoustic streaming to regulate and move aggregated particles.

SHAABAN M et al[116] used a phase-resolved PIV approach to detect flow through acoustic resonance connected to three irregularly spaced inline cylinders. Strouhal demonstrated several self-sustaining flow oscillations around the analyzed configuration. To illuminate the test portion in the center, the PIV system employed a double-pulsed Nd: YAG laser with a wavelength of 532 nm and pulse energy of 200 mJ at a frequency of 15 Hz. They synchronized the laser with a 12-bit digital CMOS camera of resolution 1 920×1 200 pixels to record consecutive frames. They used propylene glycol fogging particles as seeding particles with an average diameter of 10 μm. Results show a significant difference between the flow field with acoustic resonance and without acoustic resonance.

2.8 Geology

For weather forecasts and the quantitative description of atmospheric circulations, it′s crucial to the formation of motion vectors, especially in places where radiosondes can′t be used. Many studies anticipate hurricane track forecasts using Numerical Weather Prediction (NWP) and tropical cyclone strength[121, 160-164].

CHUANG W L et al[118] employed the PIV approach to estimate Atmospheric Motion Vectors (AMVs) from infrared window channel geostationary satellite pictures. The geostationary satellite Himawari-8 is a new generation satellite with more observation channels and higher frequency. The AMVs were generated by PIV cross-correlation using consecutive images from the Multifunctional Transport Satellite series (MTSAT-2) with increased accuracy and widespread distribution over eastern Asia. The AMVs produced by PIV were compared with radiosonde data, wind fields generated from NWP analysis, and the operating system from the Japan Meteorological Agency′s (JMA) Meteorological Satellite Center (MSC) or JMA/MSC. The comparison of these results with other techniques found that a very small error occurred, so the PIV technique will be a new alternative to existing methods to find AMVs.

PATEL A et al[120] used satellite images and the PIV approach to measure the surface ice velocity of the Chhota-Shigri glacier. Landsat (TM/ETM+) and the Advanced Spaceborne Thermal Emission and Reflection Radiometer (ASTER) were used to examine the temporal data collection of the Chhota Shigri glacier from 2009 to 2016 and 2006 to 2007. They performed PIV analysis on the same dataset using four window sizes (low, medium, high, and extremely high) using open-source software for cross-correlation. The PIV findings with a medium window size were quite similar to the previously reported data. The glacier′s accumulation zone has the lowest velocities, while the central section has the greatest velocities.

NAVES J et al[119] employed LSPIV and Structure from Motion (SfM) approaches to create a 2D shallow water model for a street-size urban drainage model. They use a full-scale urban drainage model of size 36 m^2 and generate three different intensities of rain: 30, 50, and 80 mm/h. To begin, researchers applied the SfM imaging approach to physical model gully pots and compared the findings to traditional data point recorded topography, finding minor discrepancies in the velocity distributions of drainage channel sections of a few millimeters depth. They applied the LSPIV method using Ultraviolet (UV) light of wavelength 390 nm to fluorescent the seeding particles of size 0.85 mm. They conducted this experiment in dark conditions to track the illuminated UV particles. To record the LSPIV video, two cameras (Lumix GH4) with a focal length of 28 mm and with a frame size of 3 840×2 178 pixels at a 25 Hz frequency were used. For analyzing the PIV data, the open-source PIV tool for MATLAB 'PIVLab' was used to find the velocity map[153]. For measuring

runoff velocities in urban drainage systems accurately, LSPIV is a very suitable technique.

2.9 Oceanography and water resources

Surface water resource management and control of flooding are major problems. An important hydrological parameter is river discharge. Flow measurement technologies have been used for over 100 years and must be calibrated manually, not only for the first time but regularly. New prospective approaches, such as imaging-based LSPIV and near-field remote sensing techniques, such as radar, should address challenges[124, 129-130]. Stereo-imaging LSPIV in mountain river flows can assess 3D water surface reconstruction and discharge[127]. Yeh et al[132] use adaptive LSPIV to quantify the surface velocity of river flow using a dynamically altering detection zone strategy.

JIN T et al[126] apply LSPIV in the estimation of natural river water depth and surface turbulence. The comparison of LSPIV results with Acoustic Doppler Velocimeter (ADV) results was used to validate turbulence measurement velocity and Turbulent Kinetic Energy (TKE) dissipation rate. They recorded the video with a digital camera working at a frequency of 25 frames per second for 10 minutes. For effective detection, surface foams and surface deformations owing to some short waves (capillary gravity waves) were employed as tracer particles or patterns in LSPIV implementation on the river for effective detection[122]. While utilizing classic LSPIV to establish river bathymetry and water depth requires a secondary measurement, they developed a novel approach for controlled flow to measure cross-sectional geometry using the Manning-Strickler formula to the combined observations of surface velocity and dissipation rate.

STRELNIKOVA D et al[131] used drone-based optical measurements at hydropower dams to quantify heterogeneous surface velocity fields near fish passageways via LSPIV. Dams that support the connection of habitats for riverine fish species are being built with fish passageways to reduce their ecological effect and increase the sustainability of hydropower. To record the video, a quadcopter drone (DJI Mavic Pro drone) camera with a resolution of 3 840×2 160 pixels at 25 frames per second was used. For seeding the flow, eco foam in various colors (light green, pink, azure, and yellow) was utilized as a tracer. Tracers were introduced after 40 seconds to start the recording, and after three and a half minutes, they observed the best seeding at the entrance to the fish ladder. PIVlab (popular MATLAB-based software) was used to perform data evaluation[153]. Fig. 9 illustrates a Surface Velocity Field (SVF) generated using PIV and the geographical distribution of reference values near the fishway. The results show that LSPIV, which is based on ensemble correlation, produces velocities that were in good agreement with reference values in terms of flow direction and magnitude.

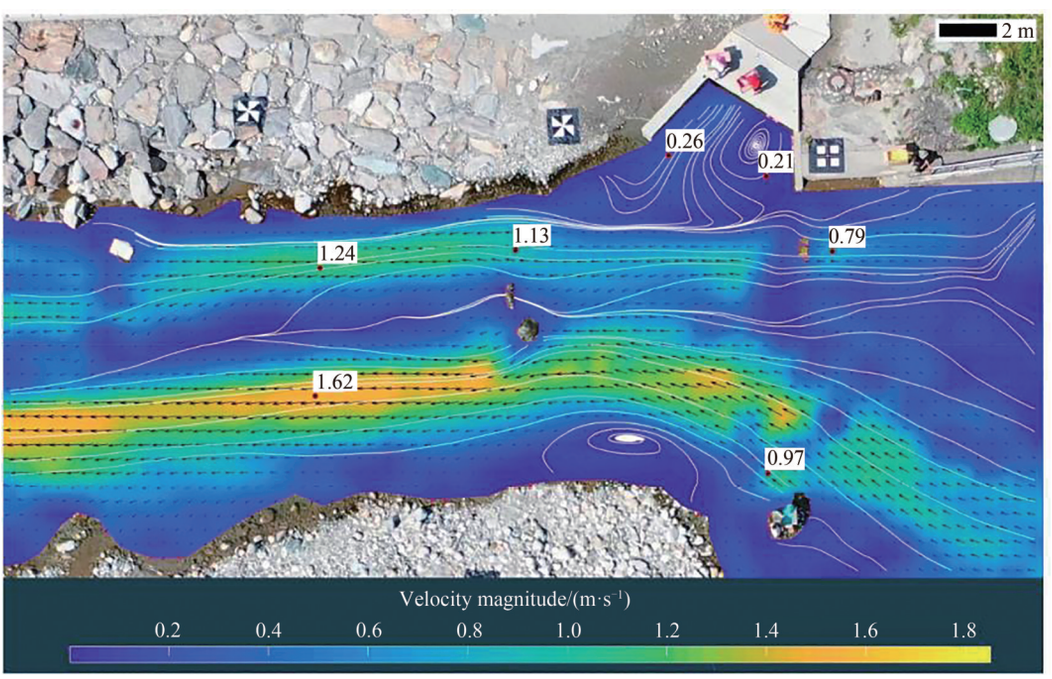

Fig. 9 A surface velocity field generated using PIV and the spatial distribution of reference measurements near the fishway[131]

LIU W C[165] created a three-axis accelerometer and LSPIV to monitor nonintrusive surface velocities in the river. To verify the accuracy, they measured surface velocities using a flow meter, LSPIV with ground control points, and a three-axis accelerometer. The LSPIV approach, in combination with a three-axis accelerometer, enhanced surface velocity measurement accuracy. The impacts of camera posture, Interrogation Area (IA), three-axis acceleration, and image quality on surface velocity measurement were investigated.

2.10 Forestry

Wood is a versatile material with a wide range of applications, so understanding its mechanical qualities is critical. When working with wood, it is critical to understand the qualities that contrast. When applying a load to a wood sample, a variation in physical attributes reflects a change in its behavior along its axis[135-136, 138].

PEREIRA R A et al[137] demonstrate a displacement map and static bending test behavior of *Pinus oocarpa* and *Eucalyptus grandis* wood samples, plywood panels, Laminated Veneer Lumber (LVL), and Oriented Strand Board (OSB) using the PIV approach. A remotely controlled professional digital camera (CANON EOS Rebel t3) was used to get PIV images perpendicular to the sample. The open-source PIV algorithm in GNU Octave was used to determine the displacements of subsequent images from the reference image. The results show that the PIV technique effectively alternates those traditionally used for conventional analysis and standardized techniques.

GUEDES T O et al[133-134] applied the PIV technique to wood for the investigation of mechanical and structural properties to estimate Young′s modulus independently of the wood density. Using the PIV technique, universal testing equipment, and transversal vibration, wood specimens from Cedrela spp. and Eucalyptus cloeziana were studied to evaluate and correlate their Young modulus. From the start of the test to the point right before the specimen broke, images were taken every 30 seconds for PIV. After that, Young′s Modulus was calculated using free software for displacement measurement with the PIV algorithm.

2.11 Crowd monitoring

For traffic management and public safety purposes, it′s very important to analyze pedestrian videos continuously and intelligently. Even with state-of-the-art approaches, intelligent pedestrian surveillance has several limitations to generate relevant information and automating high-density pedestrian movement using Closed-Circuit Television (CCTV) images[140].

BAQUI M et al[139] used the PIV approach to analyze velocities from high-density pedestrian events to learn about pedestrian flow dynamics at Mecca′s Great Mosque, which is quite crowded. They take a sequence of two or more pictures from a closed-circuit conventional television camera and collect flow parameters such as direction and speed. Open-source packages OpenPIV[166], PIVlab[167], and MatPIV[168] were used to estimate the velocities of the pedestrian flow. Despite the low frame rate, a correlation surface generated from crowd images was able to produce displacement peaks in two consecutive frames. The PIV processed result for pedestrian velocities and velocity vectors was obtained from a set of images. These vectors indicate the circular motion of the crowd anti-clockwise, during processing of automatic background subtraction and a moderate density of 4-6 persons per square meter.

2.12 Mining mineral processing

Material extraction and recycling are becoming increasingly crucial as environmental protection demands rise and natural resources become limited. In the mineral industry, flotation is a crucial process. Because of the advancement of large-scale flotation cells, optimizing large-scale flotation cells has become increasingly important in increasing metallurgical performance and reducing energy consumption. SHI S et al[142] investigated the impeller angle in a flotation cell experimentally and computationally using PIV and CFD, respectively.

GUO X H et al[141] employed the PIV approach to evaluate the Stirring Settler′s efficiency (which is used to separate minerals and materials in the liquid phase) and compared the findings with CFD-PBM simulations to quantify the flow field at several agitation speeds. The simulated results were closely matched with experimental PIV data, showing that organic phase droplets had a high collision efficiency and that an adequate agitation speed can speed up the separation process. The breakage of the organic phase droplets because of the shear stress of the fluid when a very large agitating speed was applied also decreased the separation efficiency.

3 Conclusion and perspectives

The PIV approach based on illuminated tracer particles has advanced to a high level of development, starting in the laboratory and spreading to a wide range of professional and industrial applications during the previous few decades.

1) The advancement of lasers, cameras, and fiber-based endoscopes dramatically enhanced PIV technology, allowing it to monitor especially and temporally defined velocity fields and capture instantaneous processes.

2) To gain insight into the flow field and even into the control of processes, PIV could be combined with other optical and spectroscopic diagnostics for the measurement of multiple parameters simultaneously, such as velocity, temperature, or species concentration.

3) Through acceptable expansion and summarization, PIV data can be applied to numerical modeling under a broad variety of circumstances, while validated numerical simulations can be utilized to test the accuracy and capability of PIV techniques.

The future of PIV measurements will include more elegant research items and more practical applications. The PIV system design, optical arrangement, the testing environment′s complex limits, and other factors should be considered. PIV measurements′ industrial and applied uses will increase their applicability and capacity.

1) As the quality of PIV images improves, rapid and automated algorithms for industrial applications face new hurdles. Efforts are continually being made to improve the processing speed of PIV images by combining smart software with complicated hardware.

2) Meanwhile, complementary developments of experimental methods, such as 3D-PIV and HPIV, increase the complexity of the images to be analyzed.

3) It should be effective, easy, and convenient for processing, analyzing, and storing large amounts of PIV data in a short amount of time.

References

[1] ADRIAN R J. Scattering particle characteristics and their effect on pulsed laser measurements of fluid flow: speckle velocimetry vs particle image velocimetry[J]. Applied Optics, 1984, 23(11): 1690-1691.

[2] ADRIAN R J. Twenty years of particle image velocimetry[J]. Experiments in Fluids, 2005, 39(2): 159-169.

[3] BARKER D B, FOURNEY M E. Measuring fluid velocities with speckle patterns[J]. Optics Letters, 1977, 1(4): 135-137.

[4] DUDDERAR T D, SIMPKINS P G. Laser speckle photography in a fluid medium[J]. Nature, 1977, 270(5632): 45-47.

[5] GROUSSON R, MALLICK S. Study of flow pattern in a fluid by scattered laser light[J]. Applied Optics, 1977, 16(9): 2334-2336.

[6] ADRIAN L, ADRIAN RJ, WESTERWEEL J. Particle image velocimetry[M]. Cambridge University Press, 2011.

[7] RAFFEL M, WILLERT CE, SCARANO F, et al. Particle image velocimetry: a practical guide[M]. Springer, 2018.

[8] AKBARI G, MONTAZERIN N. Subgrid-scale stress parameterization for anisotropic turbomachinery flow as deduced from stereoscopic particle image velocimetry measurements[J]. Journal of the Brazilian Society of Mechanical Sciences and Engineering, 2019, 41(8): 1-19.

[9] CAPONE A, ALVES PEREIRA F, MAIOCCHI A, et al. Analysis of the hull wake of a twin-screw ship in steady drift by borescope stereo particle image velocimetry[J]. Applied Ocean Research, 2019, 92: 101914.

[10] EL-ADAWY M, HEIKAL M R, AZIZ A R. Stereoscopic particle image velocimetry measurements and proper orthogonal decomposition analysis of the in-cylinder flow of gasoline direct injection engine[J]. Journal of Energy Resources Technology, 2019, 141(4): 042204-042217.

[11] HIRATSUKA M, ITO S, MIYASAKA K, et al. Stereo three-dimensional particle image velocimetry measurement and aerodynamic force analysis of non-spinning soccer balls[J]. Proceedings of the Institution of Mechanical Engineers, Part P: Journal of Sports Engineering and Technology, 2020: 146-153.

[12] HITIMANA E, FOX R O, HILL J C, et al. Experimental characterization of turbulent mixing performance using simultaneous stereoscopic particle image velocimetry and planar laser-induced fluorescence[J]. Experiments in Fluids, 2019, 60(2): 1-13.

[13] KIM D, KIM D, KIM M, et al. Velocity field measurement on natural convection inside an automotive headlamp using time-resolved stereoscopic particle image velocimetry[J]. International Journal of Heat and Fluid Flow, 2019, 77: 19-30.

[14] WEN X, LIU J, KIM D, et al. Study on three-dimensional flow structures of a sweeping jet using time-resolved stereo particle image velocimetry[J]. Experimental Thermal and Fluid Science, 2020, 110: 109945-109956.
[15] JACOBI G, THILL C H, VAN'T VEER R, et al. Analysis of the influence of an interceptor on the transom flow of a fast ship by pressure reconstruction from stereoscopic scanning PIV[J]. Ocean Engineering, 2019, 181: 281-292.
[16] NGUYEN Y N, KABINEJADIAN F, ISMAIL M, et al. Ex vivo assessment of bicuspidization repair in treating severe functional tricuspid regurgitation: a stereo-scopic PIV study[J]. Scientific Reports, 2019, 9(1): 1-13.
[17] VOORNEVELD J, KEIJZER L B H, STRACHINARU M, et al. High-frame-rate echo-particle image velocimetry can measure the high-velocity diastolic flow patterns[J]. Circ Cardiovasc Imaging, 2019, 12(4): e008856.
[18] VOORNEVELD J, SAAID H, SCHINKEL C, et al. 4-D echo-particle image velocimetry in a left ventricular phantom[J]. Ultrasound Med Biol, 2020, 46(3): 805-817.
[19] AGUIRRE-PABLO A A, ALARFAJ M K, LI E Q, et al. Tomographic particle image velocimetry using smartphones and colored shadows[J]. Scientific Reports, 2017, 7(1): 3714.
[20] KHASHEHCHI M, HARUN Z. Accuracy of tomographic particle image velocimetry data on a turbulent round jet[J]. International Journal of Heat and Fluid Flow, 2019, 77: 61-72.
[21] ROLOFF C, STUCHT D, BEUING O, et al. Comparison of intracranial aneurysm flow quantification techniques: standard PIV vs stereoscopic PIV vs tomographic PIV vs phase-contrast MRI vs CFD[J]. Journal of NeuroInterventional Surgery, 2019, 11(3): 275-282.
[22] WANG C, GAO Q, WANG J, et al. Experimental study on dominant vortex structures in near-wall region of turbulent boundary layer based on tomographic particle image velocimetry[J]. Journal of Fluid Mechanics, 2019, 874: 426-454.
[23] ZHANG B, LUAN B, DONG J, et al. Simultaneous deflection tomography and PIV measurements of non-premixed combustion[J]. Optics and Lasers in Engineering, 2020, 127: 105944-105951.
[24] MATT S, NOOTZ G, HELLMAN S, et al. Effects of optical turbulence and density gradients on particle image velocimetry[J]. Scientific Reports, 2020, 10(1): 2130-2141.
[25] FILATYEV S, THARIYAN M, LUCHT R, et al. Simultaneous stereo particle image velocimetry and double-pulsed planar laser-induced fluorescence of turbulent premixed flames[J]. Combustion and Flame, 2007, 150(3): 201-209.
[26] ZHANG Z, SETH D, ARTHAM S K, et al. Time-resolved flowfield measurements of momentum-driven pulsed transient jets[J]. AIAA Journal, 2018, 56(4): 1434-1446.
[27] LEWANDOWSKI B, FERTIG M, KREKE G, et al. Analysis of wake structures in bubbly flowsusing Particle Image Velocimetry (PIV)[J]. Chemical and Process Engineering, 2019, 40(1): 49-55.
[28] DENG K, ZHONG Y, WANG M, et al. Effects of acoustic excitation on the combustion instability of hydrogen-methane lean premixed swirling flames[J]. ACS Omega, 2020, 5(15): 8744-8753.
[29] KÄUFER T, KÖNIG J, CIERPKA C. Stereoscopic PIV measurements using low-cost action cameras[J]. Experiments in Fluids, 2021, 62(3): 1-16.
[30] FRUCHTEL G, HASSEL E P, JANICKA J. Turbulent length scales in a swirling flame[M]. Burgess AR, Dryer FL, 1996: 195-202.
[31] HASSEL E P, LINOW S. Laser diagnostics for studies of turbulent combustion [J]. Measurement Science and Technology, 2000, 11(2): R37-R57.
[32] TUTTLE S G, CARTER C D, HSU K Y. Particle image velocimetry in a nonreacting and reacting high-speed cavity[J]. Journal of Propulsion and Power, 2014, 30(3): 576-591.
[33] DAGHRAH M, WANG Z, LIU Q, et al. Characterization of oil flow within radial cooling ducts of disc type transformer windings using particle image velocimetry[J]. IEEE Electrical Insulation Magazine, 2019, 35(2): 9-17.
[34] AHMADI F, EBRAHIMIAN M, SANDERS R S, et al. Particle image and tracking velocimetry of solid-liquid turbulence in a horizontal channel flow[J]. International Journal of Multiphase Flow, 2019, 112: 83-99.
[35] LI L, YAN H. A robust filtering algorithm based on the estimation of tracer visibility and stability for large scale particle image velocimetry[J]. Flow Measurement and Instrumentation, 2022: 102204-102215.
[36] CLÉMENT S A, ANDRÉ M A, BARDET P M. Multi-spatio-temporal scales PIV in a turbulent buoyant jet discharging in a linearly stratified environment[J]. Experimental Thermal and Fluid Science, 2021, 129: 110429.
[37] WESTERWEEL J, DABIRI D, GHARIB M. The effect of a discrete window offset on the accuracy of cross-correlation analysis of digital PIV recordings[J]. Experiments in Fluids, 1997, 23(1): 20-28.
[38] WERELEY S T, MEINHART C D. Second-order accurate particle image velocimetry[J]. Experiments in Fluids, 2001, 31(3): 258-268.
[39] GUI L, WERELEY S. A correlation-based continuous window-shift technique to reduce the peak-locking effect in digital PIV image evaluation[J]. Experiments in Fluids, 2002, 32(4): 506-517.
[40] SCARANO F, RIETHMULLER M L. Iterative multigrid approach in PIV image processing with discrete window offset[J]. Experiments in Fluids, 1999, 26(6): 513-523.

[41] HUANG H, FIEDLER H, WANG J. Limitation and improvement of PIV. I: Limitation of conventional techniques due to deformation of particle image patterns[J]. Experiments in Fluids, 1993, 15(3): 168-174.
[42] JAMBUNATHAN K, JU X, DOBBINS B, et al. An improved cross correlation technique for particle image velocimetry[J]. Measurement Science and Technology, 1995, 6(5): 507.
[43] WILLERT C E, GHARIB M. Digital particle image velocimetry[J]. Experiments in Fluids, 1991, 10(4): 181-193.
[44] ECKSTEIN A, VLACHOS P P. Assessment of advanced windowing techniques for digital particle image velocimetry (DPIV)[J]. Measurement Science and Technology, 2009, 20(7): 075402.
[45] HART D P. Super-resolution PIV by recursive local-correlation[J]. Journal of Visualization, 2000, 3(2): 187-194.
[46] ERGIN F G. An automatic static masking technique using particle image velocimetry image ensembles[J]. Experimental Thermal and Fluid Science, 2021, 128: 110431-110439.
[47] ALEXANDER B F, NG K C. Elimination of systematic error in subpixel accuracy centroid estimation[J]. Optical Engineering, 1991, 30(9): 1320-1332.
[48] MORGAN J S, SLATER D, TIMOTHY J G, et al. Centroid position measurements and subpixel sensitivity variations with the MAMA detector[J]. Applied Optics, 1989, 28(6): 1178-1192.
[49] LOURENCO L, KROTHAPALLI A. On the accuracy of velocity and vorticity measurements with PIV[J]. Experiments in Fluids, 1995, 18(6): 421-428.
[50] RÖSGEN T. Optimal subpixel interpolation in particle image velocimetry[J]. Experiments in Fluids, 2003, 35(3): 252-256.
[51] CHEN J, KATZ J. Elimination of peak-locking error in PIV analysis using the correlation mapping method[J]. Measurement Science and Technology, 2005, 16(8): 1605.
[52] CHRISTENSEN K. The influence of peak-locking errors on turbulence statistics computed from PIV ensembles[J]. Experiments in Fluids, 2004, 36(3): 484-497.
[53] FINCHAM A, SPEDDING G. Low cost, high resolution DPIV for measurement of turbulent fluid flow[J]. Experiments in Fluids, 1997, 23(6): 449-462.
[54] PRASAD A, ADRIAN R, LANDRETH C, et al. Effect of resolution on the speed and accuracy of particle image velocimetry interrogation[J]. Experiments in Fluids, 1992, 13(2-3): 105-116.
[55] WESTERWEEL J. Effect of sensor geometry on the performance of PIV interrogation[M]. Laser Techniques Applied to Fluid Mechanics, Springer, 2000: 37-55.
[56] GUI L, MERZKIRCH W, FEI R. A digital mask technique for reducing the bias error of the correlation-based PIV interrogation algorithm[J]. Experiments in Fluids, 2000, 29(1): 30-35.
[57] LIAO Q, COWEN E A. An efficient anti-aliasing spectral continuous window shifting technique for PIV[J]. Experiments in Fluids, 2005, 38(2): 197-208.
[58] NOGUEIRA J, LECUONA A, RODRIGUEZ P. Identification of a new source of peak locking, analysis and its removal in conventional and super-resolution PIV techniques[J]. Experiments in Fluids, 2001, 30(3): 309-316.
[59] HUANG H, DABIRI D, GHARIB M. On errors of digital particle image velocimetry[J]. Measurement Science and Technology, 1997, 8(12): 1427.
[60] ROHALY J, FRIGERIO F, HART D. Reverse hierarchical PIV processing[J]. Measurement Science and Technology, 2002, 13(7): 984.
[61] NOBACH H, DAMASCHKE N, TROPEA C, et al. Cross sectional area difference method for backscatter particle sizing [C]. Proceedings of the 12th International Symposium on Applications of Laser Techniques to Fluid Mechanics, 2002.
[62] NOGUEIRA J, LECUONA A, RODRIGUEZ P. Local field correction PIV: on the increase of accuracy of digital PIV systems[J]. Experiments in Fluids, 1999, 27(2): 107-116.
[63] FINCHAM A, DELERCE G. Advanced optimization of correlation imaging velocimetry algorithms[J]. Experiments in Fluids, 2000, 29(1): S013-S022.
[64] HUANG H, FIEDLER H, WANG J. Limitation and improvement of PIV[J]. Experiments in Fluids, 1993, 15(4-5): 263-273.
[65] LECORDIER B. Etude de l'interaction de la propagation d'une flamme prémélangée avec le champ aérodynamique, par association de la tomographie laser et de la vélocimétrie par images de particules[T]. Rouen, 1997.
[66] SCARANO F. Iterative image deformation methods in PIV[J]. Measurement Science and Technology, 2001, 13(1): R1.
[67] SCARANO F, RIETHMULLER ML. Advances in iterative multigrid PIV image processing[J]. Experiments in Fluids, 2000, 29(1): S051-S060.
[68] ASTARITA T. Analysis of velocity interpolation schemes for image deformation methods in PIV[J]. Experiments in Fluids, 2008, 45(2): 257-266.
[69] SCARANO F. Laser photothermal velocimeter by compulsorily operating point locked optical-deflection-probe [C]. 12th International Symposium on Applications of Laser Techniques, 2004.

[70] SCHRIJER F, SCARANO F. Effect of predictor - corrector filtering on the stability and spatial resolution of iterative PIV interrogation[J]. Experiments in Fluids, 2008, 45(5): 927-941.
[71] TOKUMARU P, DIMOTAKIS P. Image correlation velocimetry[J]. Experiments in Fluids, 1995, 19(1): 1-15.
[72] NOBACH H, BODENSCHATZ E. Limitations of accuracy in PIV due to individual variations of particle image intensities[J]. Experiments in Fluids, 2009, 47(1): 27-38.
[73] SCIACCHITANO A. Uncertainty quantification in particle image velocimetry[J]. Measurement Science and Technology, 2019, 30(9): 0920001.
[74] NOGUEIRA J, LEGRAND M, JIMENEZ R, et al. Peak-locking full characterization: PIV error assessment and velocity ensemble measurement correction[J]. Measurement Science and Technology, 2021, 32(11): 114005.
[75] ANGELBERGER C, ZHAO F, LIU M, et al. Multi-plane time-resolved Particle Image Velocimetry (PIV) flow field measurements in an optical Spark-Ignition Direct-Injection (SIDI) engine for Large-Eddy Simulation (LES) model validations[J]. Oil & Gas Science and Technology, 2019, 74: 52-70.
[76] BRADLEY D, LAWES M, MORSY M E. Flame speed and particle image velocimetry measurements of laminar burning velocities and Markstein numbers of some hydrocarbons[J]. Fuel, 2019, 243: 423-432.
[77] BREND M A, DENMAN P A, CARROTTE J F. Volumetric PIV measurement for capturing the port flow characteristics within annular gas turbine combustors[J]. Experiments in Fluids, 2020, 61(4): 1-17.
[78] JEVNIKAR S, SIDDIQUI K. Investigation of the influence of heat source orientation on the transient flow behavior during PCM melting using particle image velocimetry[J]. Journal of Energy Storage, 2019, 25: 100825.
[79] OSTOVAN Y, AKPOLAT M T, UZOL O. Experimental investigation of the effects of winglets on the tip vortex behavior of a model horizontal axis wind turbine using particle image velocimetry[J]. Journal of Solar Energy Engineering, 2019, 141(1): 011006-011018.
[80] WU A, KEUM S, GREENE M, et al. Comparison of near-wall flow and heat transfer of an internal combustion engine using particle image velocimetry and computational fluid dynamics[J]. Journal of Energy Resources Technology, 2019, 141(12): 122202-122201.
[81] ZHANG C, JU H, ZHANG D, et al. PIV measurement and numerical investigation on flow characteristics of simulated fast reactor fuel subassembly[J]. Nuclear Engineering and Technology, 2020, 52(5): 897-907.
[82] ZHANG Z, MA H. Particle Image Velocimetry (PIV) investigation of blade and purge flow impacts on inter-stage flow field in a research turbine[J]. Energies, 2019, 12(7): 1240-1260.
[83] TOMBUL H, OZBAYOGLU A M, OZBAYOGLU M E. Computational intelligence models for PIV based particle (cuttings) direction and velocity estimation in multi-phase flows[J]. Journal of Petroleum Science and Engineering, 2019, 172: 547-558.
[84] ZHANG Z, MA H. Application of phase-locked PIV technique to the measurements of flow field in a turbine stage[J]. Journal of Thermal Science, 2020, 29(3): 784-792.
[85] CRESSALL R, SCHAAP R, NEAL D R, et al. Accuracy of volumetric flow rate inflow/outflow measurement by integrating PIV velocity fields[J]. Measurement Science and Technology, 2020, 31(11): 115303.
[86] MURAKAMI M, TAKADA S. PIV measurement of flow field generated during noisy film boiling in saturated He II[J]. Cryogenics, 2020, 108: 103083.
[87] ZHANG J, BHATTACHARYA S, VLACHOS P P. Using uncertainty to improve pressure field reconstruction from PIV/PTV flow measurements[J]. Experiments in Fluids, 2020, 61(6): 1-20.
[88] VARON E, AIDER J L, EULALIE Y, et al. Adaptive control of the dynamics of a fully turbulent bimodal wake using real-time PIV[J]. Experiments in Fluids, 2019, 60(8): 1-21.
[89] BREIMAN R F, COSMAS L, NJENGA M K, et al. Severe acute respiratory infection in children in a densely populated urban slum in Kenya, 2007-2011[J]. Bmc Infectious Diseases, 2015, 15: 1-11.
[90] LI G, CHEN Q, LIU Y. Experimental study on dynamic structure of propeller tip vortex[J]. Polish Maritime Research, 2020, 27(2): 11-18.
[91] LIEW C V, WANG L K, HENG P W S. Development of a visiometric process analyzer for real-time monitoring of bottom spray fluid-bed coating[J]. Journal of Pharmaceutical Sciences, 2010, 99(1): 346-356.
[92] MILLER R M, ZHANG X, MAXWELL A D, et al. Bubble-induced color doppler feedback for histotripsy tissue fractionation[J]. IEEE Transactions on Ultrasonics Ferroelectrics and Frequency Control, 2016, 63(3): 408-419.
[93] MOMEY F, COUTARD J G, BORDY T, et al. Dynamics of cell and tissue growth acquired by means of extended field of view lensfree microscopy[J]. Biomedical Optics Express, 2016, 7(2): 512-524.
[94] STUMPF A, AUGEREAU E, BONNIER J, et al. Photogrammetric discharge monitoring of torrential rivers[J]. Houille Blanche-Revue Internationale De L Eau, 2018(5-6): 66-74.
[95] SAXTON-FOX T, DING L, SMITS A, et al. Coherent structure deformation in a turbulent pipe flow with a spatially-developing pressure gradient [J]. 11th International Symposium on Turbulence and Shear Flow Phenomena, 2019.

[96] FUJIWARA A, DANMOTO Y, HISHIDA K, et al. Bubble deformation and flow structure measured by double shadow images and PIV/LIF[J]. Experiments in Fluids, 2004, 36(1): 157-165.
[97] AL-MUHAMMAD J, TOMAS S, AIT-MOUHEB N, et al. Experimental and numerical characterization of the vortex zones along a labyrinth milli-channel used in drip irrigation[J]. International Journal of Heat and Fluid Flow, 2019, 80: 108500.
[98] BAI R, ZHU D, CHEN H, et al. Laboratory study of secondary flow in an open channel bend by using PIV[J]. Water, 2019, 11(4): 659-673.
[99] YOON J S, PARK J H, CHO Y K, et al. Experiments on efficiency review of new-type screens for waste treatment in the drainage canal[J]. Journal of Coastal Research, 2019, 91(sp1): 266.
[100] SHIONO K, MUTO Y, KNIGHT DW, et al. Energy losses due to secondary flow and turbulence in meandering channels with overbank flows[J]. Journal of Hydraulic Research, 1999, 37(5): 641-664.
[101] AVELAR A H D F, STÓFEL M A G E, VIEIRA G D, et al. Analysis of leaflet flutter in biological prosthetic heart valves using PIV measurements[J]. Acta Scientiarum Technology, 2019, 42: e41746.
[102] HO W H, TSHIMANGA I J, NGOEPE M N, et al. Evaluation of a desktop 3D printed rigid refractive-indexed-matched flow phantom for PIV measurements on cerebral aneurysms[J]. Cardiovasc Eng Technol, 2020, 11(1): 14-23.
[103] LI Y, VERRELLI D I, YANG W, et al. A pilot validation of CFD model results against PIV observations of haemodynamics in intracranial aneurysms treated with flow-diverting stents[J]. Journal of Biomechanics, 2020, 100: 109590.
[104] THIELICKE W. The flapping flight of birds[T]. Cambridge University Press, 2014.
[105] ZHOU X, PAPADOPOULOU V, LEOW C H, et al. 3-D flow reconstruction using divergence-free interpolation of multiple 2-D contrast-enhanced ultrasound particle imaging velocimetry measurements[J]. Ultrasound Med Biol, 2019, 45(3): 795-810.
[106] ZHU G, WEI Y, YUAN Q, et al. PIV investigation of the flow fields in subject-specific vertebro-basilar (VA-BA) junction[J]. Biomed Eng Online, 2019, 18(1): 1-19.
[107] BOUILLOT P, BRINA O, OUARED R, et al. Particle imaging velocimetry evaluation of intracranial stents in sidewall aneurysm: hemodynamic transition related to the stent design[J]. Plos One, 2014, 9(12): e113762.
[108] PARK H, YEOM E, LEE S J. X-ray PIV measurement of blood flow in deep vessels of a rat: an in vivo feasibility study [J]. Scientific Reports, 2016, 6(1): 1-8.
[109] GAO Y, YANG XY, FU C, et al. 10 kHz simultaneous PIV/PLIF study of the diffusion flame response to periodic acoustic forcing[J]. Applied Optics, 2019, 58(10): E112-E120.
[110] KUZUU K, HASEGAWA S. Reconstruction of an acoustic pressure field in a resonance tube by particle image velocimetry[J]. The Journal of the Acoustical Society of America, 2015, 138(5): 3160-3168.
[111] LIOU Y S, KANG X J, TIEN W H. Particle aggregation and flow patterns induced by ultrasonic standing wave and acoustic streaming: An experimental study by PIV and PTV[J]. Experimental Thermal and Fluid Science, 2019, 106: 78-86.
[112] LODERMEYER A, TAUTZ M, BECKER S, et al. Aeroacoustic analysis of the human phonation process based on a hybrid acoustic PIV approach[J]. Experiments in Fluids, 2017, 59(1): 1-15.
[113] MISHRA S K, RANA P, SAHOO S P, et al. Characterization of dye cells for a high-repetition-rate pulsed dye laser by particle image velocimetry (PIV)[J]. Laser Physics, 2019, 29(6): 065001.
[114] O'SULLIVAN J J, ESPINOZA C J U, MIHAILOVA O, et al. Characterisation of flow behaviour and velocity induced by ultrasound using particle image velocimetry (PIV): effect of fluid rheology, acoustic intensity and transducer tip size[J]. Ultrason Sonochem, 2018, 48: 218-230.
[115] OKTAMULIANI S, KANNO N, MAEDA M, et al. Validation of echodynamography in comparison with particle-image velocimetry[J]. Ultrason Imaging, 2019, 41(6): 336-352.
[116] SHAABAN M, MOHANY A. Phase-resolved PIV measurements of flow over three unevenly spaced cylinders and its coupling with acoustic resonance[J]. Experiments in Fluids, 2019, 60(4): 1-14.
[117] ISLAM R, SHAABAN M, MOHANY A. Phase-Locked PIV measurements of vortex shedding characteristics downstream of straight circular finned cylinders during acoustic resonance[C]. Proceedings of the Asme Pressure Vessels and Piping Conference, 2019.
[118] W-LCHUANG, C-BCHOU, CHANG K-A, et al. Atmospheric motion vectors derived from an infrared window channel of a geostationary satellite using particle image velocimetry[J]. Journal of Applied Meteorology and Climatology, 2019, 58(2): 199-211.
[119] NAVES J, ANTA J, PUERTAS J, et al. Using a 2D shallow water model to assess Large-Scale Particle Image Velocimetry (LSPIV) and Structure from Motion (SfM) techniques in a street-scale urban drainage physical model[J]. Journal of Hydrology, 2019, 575: 54-65.

[120] PATEL A, DHARPURE J K, SNEHMANI, et al. Estimating surface ice velocity on Chhota Shigri glacier from satellite data using Particle Image Velocimetry (PIV) technique[J]. Geocarto International, 2017, 34(4): 335-347.
[121] BERGER H, LANGLAND R, VELDEN CS, et al. Impact of enhanced satellite-derived atmospheric motion vector observations on numerical tropical cyclone track forecasts in the western north pacific during TPARC/TCS-08[J]. Journal of Applied Meteorology and Climatology, 2011, 50(11): 2309-2318.
[122] BENETAZZO A, GAMBA M, BARBARIOL F. Unseeded large scale PIV measurements corrected for the capillary-gravity wave dynamics[J]. Rendiconti Lincei, 2017, 28(2): 393-404.
[123] ASAD SMSBIN, LUNDSTRÖM T S, ANDERSSON A G, et al. Wall shear stress measurement on curve objects with PIV in connection to benthic fauna in regulated rivers[J]. Water, 2019, 11(4): 650.
[124] COSTA J E, CHENG R T, HAENI F P, et al. Use of radars to monitor stream discharge by noncontact methods[J]. Water Resources Research, 2006, 42(7): 1-14.
[125] GAO X, SONG Q, SUN B, et al. PIV experimental study on the flow characteristics upstream of a floating intake in nonlinear stratified ambient conditions[J]. Environmental Fluid Mechanics, 2019, 19(4): 1005-1024.
[126] JIN T, LIAO Q. Application of large scale PIV in river surface turbulence measurements and water depth estimation[J]. Flow Measurement and Instrumentation, 2019, 67: 142-152.
[127] LI W, LIAO Q, RAN Q. Stereo-imaging LSPIV (SI-LSPIV) for 3D water surface reconstruction and discharge measurement in mountain river flows[J]. Journal of Hydrology, 2019, 578: 124099.
[128] LV M, MAO Y, XIA M, et al. Particle image velocimetry and numerical studies of artificial upwelling via differential heating in open surroundings[J]. Revista Internacional de Contaminación Ambiental, 2019, 35(esp01): 53-63.
[129] MUSTE M, FUJITA I, HAUET A. Large-scale particle image velocimetry for measurements in riverine environments[J]. Water Resources Research, 2008, 44: 1-14.
[130] RAN Q H, LI W, LIAO Q, et al. Application of an automated LSPIV system in a mountainous stream for continuous flood flow measurements[J]. Hydrological Processes, 2016, 30(17): 3014-3029.
[131] STRELNIKOVA D, PAULUS G, KÄFER S, et al. Drone-based optical measurements of heterogeneous surface velocity fields around fish passages at hydropower dams[J]. Remote Sensing, 2020, 12(3): 384-408.
[132] YEH M T, Y-NCHUNG, HUANG Y X, et al. Applying adaptive LS-PIV with dynamically adjusting detection region approach on the surface velocity measurement of river flow[J]. Computers & Electrical Engineering, 2019, 74: 466-482.
[133] ZHAO D, GUO C, WU T, et al. Hydrodynamic interactions between bracket and propeller of podded propulsor based on particle image velocimetry test[J]. Water, 2019, 11(6): 1142.
[134] GUEDES T O, PEREIRA R A, RIVIEIRA F P, et al. Particle image velocimetry for estimating the Young's modulus of wood specimens[J]. Cerne, 2019, 25(2): 240-245.
[135] MELANDER O, RASMUSON A. PIV measurements of velocities and concentrations of wood fibres in pneumatic transport[J]. Experiments in Fluids, 2004, 37(2): 293-300.
[136] PEREIRA R A, GOMES F C, BRAGA JUNIOR R A, et al. Analysis of elasticity in woods submitted to the static bending test using the particle image velocimetry (PIV) technique[J]. Engenharia Agricola, 2018, 38(2): 159-165.
[137] PEREIRA R A, GOMES F C, BRAGA JÚNIOR R A, et al. Displacement measurement in sawn wood and wood panel beams using particle image velocimetry[J]. Cerne, 2019, 25(1): 110-118.
[138] SOUZA T M, CONTADO EWNF, BRAGA R A, et al. Non-destructive technology associating PIV and Sunset laser to create wood deformation maps and predict failure[J]. Biosystems Engineering, 2014, 126: 109-116.
[139] BAQUI M, LOHNER R. PedPIV: Pedestrian velocity extraction from particle image velocimetry [J]. IEEE Transactions on Intelligent Transportation Systems, 2020, 21(2): 580-589.
[140] BAQUI M, SAMAD M D, LÖHNER R. A novel framework for automated monitoring and analysis of high density pedestrian flow[J]. Journal of Intelligent Transportation Systems, 2019: 1-13.
[141] GUO X H, ZHANG T A, ZHAO Q Y, et al. CFD-PBM simulation and piv measurement of liquid-liquid flow in a continuous stirring settler[J]. Jom, 2019, 71(12): 4500-4508.
[142] SHI S, ZHANG M, FAN X, et al. Experimental and computational analysis of the impeller angle in a flotation cell by PIV and CFD[J]. International Journal of Mineral Processing, 2015, 142: 2-9.
[143] FAN L, MCGRATH D, CHONG CT, et al. Laser-induced incandescence particle image velocimetry (LII-PIV) for two-phase flow velocity measurement[J]. Experiments in Fluids, 2018, 59(10): 1-14.
[144] KOKMANIAN K, SCHARNOWSKI S, SCHÄFER C, et al. Investigating the flow field dynamics of transonic shock buffet using particle image velocimetry[J]. Experiments in Fluids, 2022, 63(9): 1-14.
[145] SEO H, KIM K C. Experimental study on flow and turbulence characteristics of bubbly jet with low void fraction[J]. International Journal of Multiphase Flow, 2021: 142.
[146] KWAK, PARK, KIM, et al. Shear band characterization of clayey soils with particle image velocimetry[J]. Applied Sciences, 2020, 10(3): 1139-1155.

[147] SATO K, AKAGI H, KIRIYAMA T, et al. Large deformation analysis of ground with wall movement or shallow foundation under extremely low confining pressure using PIV[C]. Vi International Conference on Particle-Based Methods. 2019: 283-293.
[148] BLANCKAERT K, GRAF W H. Momentum transport in sharp open-channel bends[J]. Journal of Hydraulic Engineering, 2004, 130(3): 186-198.
[149] EDWARDS B F, SMITH D H. Critical wavelength for river meandering[J]. Physical Review E, 2001, 63(4): 045304.
[150] LANCASTER S T, BRAS R L. A simple model of river meandering and its comparison to natural channels[J]. Hydrological Processes, 2002, 16(1): 1-26.
[151] TAURO F, PISCOPIA R, GRIMALDI S. Streamflow observations from cameras: large-scale particle image velocimetry or particle tracking velocimetry?[J]. Water Resources Research, 2017, 53(12): 10374-10394.
[152] CORTELLESSA G, STABILE L, ARPINO F, et al. Close proximity risk assessment for SARS-CoV-2 infection[J]. Science of the Total Environment, 2021, 794: 148749.
[153] THIELICKE W, STAMHUIS E. PIVlab-towards user-friendly, affordable and accurate digital particle image velocimetry in MATLAB[J]. Journal of Open Research Software, 2014, 2(1): e30.
[154] BOUILLOT P, BRINA O, OUARED R, et al. Multi-time-lag PIV analysis of steady and pulsatile flows in a sidewall aneurysm[J]. Experiments in Fluids, 2014, 55(6): 1-11.
[155] FORD M D, NIKOLOV H N, MILNER J S, et al. PIV-measured versus CFD-predicted flow dynamics in anatomically realistic cerebral aneurysm models[J]. Journal of Biomechanical Engineering-Transactions of the Asme, 2008, 130(2): 021015.
[156] IM S, GEHEO, JEON Y J, et al. Tomographic PIV measurements of flow patterns in a nasal cavity with geometry acquisition[J]. Experiments in Fluids, 2014, 55(1): 1-18.
[157] RASCHI M, MUT F, BYRNE G, et al. CFD and PIV analysis of hemodynamics in a growing intracranial aneurysm[J]. International Journal for Numerical Methods in Biomedical Engineering, 2012, 28(2): 214-228.
[158] VAN OOIJ P, SCHNEIDERS J J, MARQUERING H A, et al. 3D cine phase-contrast MRI at 3T in intracranial aneurysms compared with patient-specific computational fluid dynamics[J]. American Journal of Neuroradiology, 2013, 34(9): 1785-1791.
[159] YAGI T, SATO A, SHINKE M, et al. Experimental insights into flow impingement in cerebral aneurysm by stereoscopic particle image velocimetry: transition from a laminar regime[J]. Journal of the Royal Society Interface, 2013, 10(82): 20121031.
[160] GOERSS J S. Impact of satellite observations on the tropical cyclone track forecasts of the navy operational global atmospheric prediction system[J]. Monthly Weather Review, 2009, 137(1): 41-50.
[161] LANGLAND R H, VELDEN C, PAULEY P M, et al. Impact of satellite-derived rapid-scan wind observations on numerical model forecasts of hurricane katrina[J]. Monthly Weather Review, 2009, 137(5): 1615-1622.
[162] VELDEN C, LEWIS W E, BRESKY W, et al. Assimilation of high-resolution satellite-derived atmospheric motion vectors: impact on HWRF forecasts of tropical cyclone track and intensity[J]. Monthly Weather Review, 2017, 145(3): 1107-1125.
[163] WU Q, WANG H Q, LIN Y J, et al. Deriving AMVs from geostationary satellite images using optical flow algorithm based on polynomial expansion[J]. Journal of Atmospheric and Oceanic Technology, 2016, 33(8): 1727-1747.
[164] WU T C, VELDEN C S, MAJUMDAR S J, et al. Understanding the influence of assimilating subsets of enhanced atmospheric motion vectors on numerical analyses and forecasts of tropical cyclone track and intensity with an ensemble kalman filter[J]. Monthly Weather Review, 2015, 143(7): 2506-2531.
[165] LIU W C, HUANG W C. Development of a three-axis accelerometer and large-scale particle image velocimetry (LSPIV) to enhance surface velocity measurements in rivers[J]. Computers & Geosciences, 2021, 155: 104866.
[166] TAYLOR Z J, GURKA R, KOPP G A, et al. Long-duration time-resolved PIV to study unsteady aerodynamics[J]. IEEE Transactions on Instrumentation and Measurement, 2010, 59(12): 3262-3269.
[167] THIELICKE W, STAMHUIS E J. PIVlab-time-resolved digital particle image velocimetry tool for MATLAB[J]. Published under the BSD License, Programmed with MATLAB, 2014, 7(0.246): R14.
[168] SVEEN J. MatPIV—the PIV toolbox for MATLAB[G]. 2006.

Recent Development and Applications of Particle Image Velocimetry from Laboratory to Industry (Invited)

Muhammad Bilal[1,2], TIAN Zhenyu[1,2]
(1 *Institute of Engineering Thermophysics, Chinese Academy of Sciences, Beijing* 100190, *China*)
(2 *University of Chinese Academy of Sciences, Beijing* 100049, *China*)

Abstract: Particle Image Velocimetry (PIV) has emerged as a major experimental technique for measuring the velocity fields of fluid flows. The approach produces quantitative representations of instantaneous flow patterns which are commonly used to help construct phenomenological models for complicated flows and validate numerical simulations. PIV analysis is beneficial in several fields of experimental fluid mechanics. Two-step processing, namely auto-correlation followed by cross-correlation, has been used as a means of examining spatio-temporal flow evolution. The vorticity measurements and estimates of the accuracy as a function of spatial resolution can be achieved. The development of PIV is linked to the gradual increase in the complexity and difficulty of measuring flow fields. PIV techniques for measurements have developed significantly and new trends have emerged. The key developments are stereoscopic PIV, tomographic PIV, large-scale PIV, micro PIV, 3D PIV, pedestrian PIV and the use of high-temporal/spatial-resolution devices. PIV has wide applications in various kinds of research fields, such as medical research, energy fuels, combustion, flow field measurement, real-time process monitoring, structure deformation, irrigation, acoustics, geology, oceanography, water resources, forestry, crowd monitoring, and mining mineral processing. To the best of our knowledge, there have been few literature reviews that comprehensively discuss industrial the aspects of PIV. This review mainly focuses on a comprehensive overview of the development of PIV in the laboratory, which needs to be implemented in industry and daily life by monitoring the real-time process for better understanding. This will lead to fast industrial processing as well as health. Using PIV to replace current analytical imaging techniques with enhanced temporal and special resolution has been discussed. In addition, it also provides a comparison between numerical simulation and previously available analytical techniques with PIV.

Key words: Particle image velocimetry; Process monitoring PIV; Applications of PIV; Flow field measurement; Crowd monitoring
OCIS Codes: 290.5850; 350.4990; 120.7250; 280.7250